Collapse phase diagram of carbon nanotubes with arbitrary number of walls. Collapse modes and macroscopic analog

Y. Magnin, F. Rondepierre, W. Cui, D.J. Dunstan, A. San-Miguel

▶ **To cite this version:**

Y. Magnin, F. Rondepierre, W. Cui, D.J. Dunstan, A. San-Miguel. Collapse phase diagram of carbon nanotubes with arbitrary number of walls. Collapse modes and macroscopic analog. Carbon, 2021, 178, pp.552-562. 10.1016/j.carbon.2021.03.031 . hal-03249488

HAL Id: hal-03249488
https://hal.science/hal-03249488

Submitted on 24 Apr 2023

HAL is a multi-disciplinary open access archive for the deposit and dissemination of scientific research documents, whether they are published or not. The documents may come from teaching and research institutions in France or abroad, or from public or private research centers.

L'archive ouverte pluridisciplinaire **HAL**, est destinée au dépôt et à la diffusion de documents scientifiques de niveau recherche, publiés ou non, émanant des établissements d'enseignement et de recherche français ou étrangers, des laboratoires publics ou privés.

Distributed under a Creative Commons Attribution - NonCommercial 4.0 International License

Version of Record: https://www.sciencedirect.com/science/article/pii/S0008622321003377
Manuscript_4fe7253c4a116c0ba6f679fe7eb32347

Collapse phase diagram of carbon nanotubes with arbitrary number of walls. Collapse modes and macroscopic analog.

Y. Magnin[a,b,*], F. Rondepierre[c], W. Cui[d], D.J. Dunstan[e], A. San-Miguel[c,**]

[a] *MIT Energy Initiative, Massachusetts Institute of Technology, Cambridge, MA, United States*
[b] *Consultant, Total@Saclay NanoInnov, 2 boulevard Thomas Gobert, 91120 Palaiseau Cedex, France.*
[c] *Univ Lyon, Université Claude Bernard Lyon 1, CNRS, Institut Lumière Matière, Campus LyonTech - La Doua, F-69622 LYON, France*
[d] *School of Physics and Electronic Engineering, Jiangsu Normal University, Xuzhou 221116,China*
[e] *School of Physics and Astronomy, Queen Mary University of London, London, E1 4NS, UK*

Abstract

Carbon nanotubes tend to collapse when their diameters exceed a certain threshold, or when a sufficiently large external pressure is applied on their walls. The radial stability of tubes has been studied in each of these cases, however a general theory able to predict collapse is still lacking. Here, we propose a simple model predicting stability limits as a function of the tube diameter, the number of walls and the pressure. The model is supported by atomistic simulations, experiments, and is used to plot collapse phase diagrams. We have identified the most stable carbon nanotube, which can

*Corresponding author
**Corresponding author
Email addresses: magnin@mit.edu (Y. Magnin), alfonso.san-miguel@univ-lyon1.fr (A. San-Miguel)

© 2021 published by Elsevier. This manuscript is made available under the CC BY NC user license
https://creativecommons.org/licenses/by-nc/4.0/

support a maximum pressure of ∼18 GPa before collapsing. The latter was identified as a multiwall tube with an internal tube diameter of ∼12nm and ∼30 walls. This maximum pressure is lowered depending on the internal tube diameter and the number of walls. We then identify a tube diameter domain in which the radial mechanical stability can be treated as equivalent to macroscopic tubes, known to be described by the canonical Lévy-Carrier law. This multiscale behavior is shown to be in good agreement with experiments on the collapse of O-rings, proposed as a simple macroscopic parallel to nanotubes in this domain.

1. Introduction

Low-dimensional carbon structures such as fullerenes, graphene, carbon nanotubes (CNT), nanocones, nano-junctions [1, 2, 3, 4, 5, 6] have profoundly changed fundamental concepts of condensed matter physics in recent decades [7]. The many associated technological breakthroughs have opened perspectives in a broad range of applications, ranging from electronics [8, 9], sensor developments [10], energy transport and storage [11, 12, 13] or biology and medical sciences such as drug delivery technology [14]. While both graphene and CNT sp^2 structures have been the focus of a large part of the research effort, there exist many hybrid structures between these two, which have been much less explored [15]. In the literature, they are referred as "collapsed nanotubes", "flattened carbon nanotubes", "closed-edge graphene nanoribbons" or "dogbones". Such structures correspond to a geometrical evolution of the CNT radial cross-section, from circular through a continuum of shapes, in which the internal walls become closer together, in at least one radial direction. The terms mentioned above are most frequently used when the distance between the internal walls in the collapse direction tends to the graphitic interlayer distance, where van der Waals interactions (vdW) have to be considered. For clarity, we will refer to this state as the "collapsed" shape, and the deviations from the circular cross-section leading to it as "collapse transition" shapes. The latter can be either first-order-like

for large tube diameters, or continuous for smaller ones [16], going through different geometries including oval, race-track or polygonal [17], all grouped in the "collapse transition" domain.

Characterizing the CNT collapse behavior is strongly motivated by the change in electronic structure from the pristine circular cross-section to the deformed or collapsed geometry [18, 19, 20, 21, 22, 23, 24]. Hence, a geometrical electronic tuning based on a shape modification may offer an interesting alternative to substitutional doping in nano-engineering design [25, 26, 27].

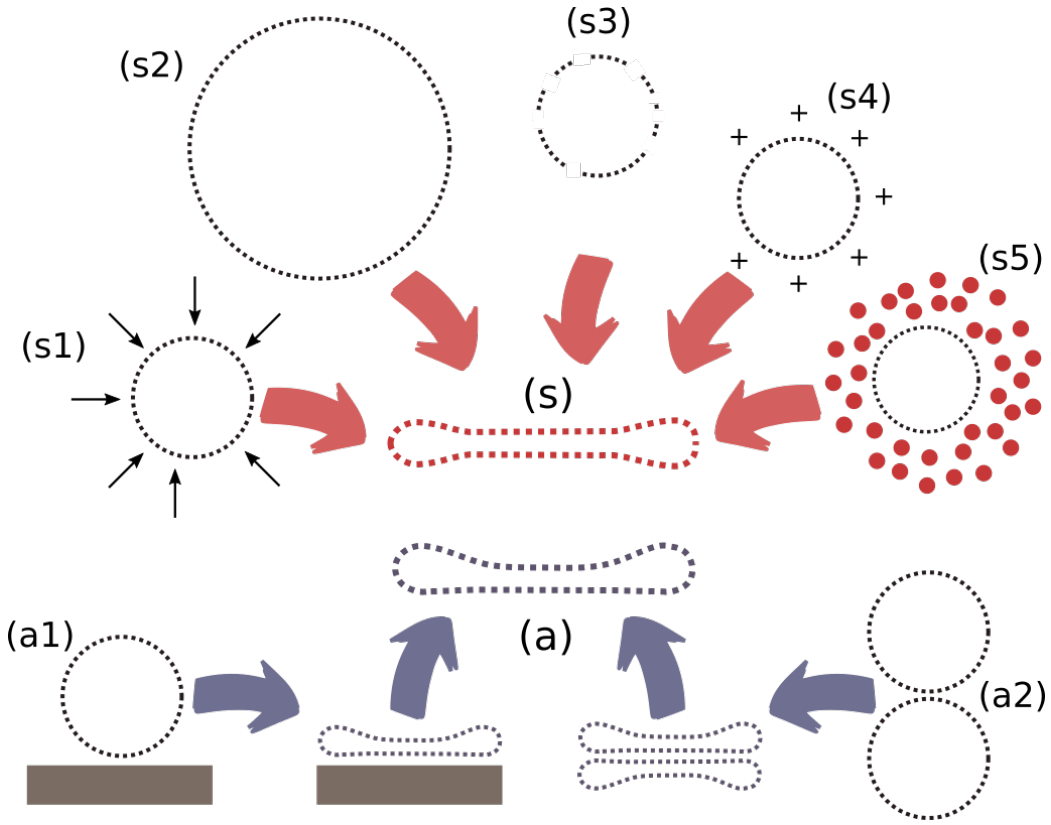

Figure 1: Scheme of the different physical mechanisms allowing the evolution of a carbon nanotube to a symmetrical collapsed structure (s): **s1** External applied pressure; **s2** Self collapse for large tube diameters; **s3** Defective tubes; **s4** Through charge injection; **s5** Through a pressure transmitting medium. Mechanisms leading to an asymmetrical collapsed structure (a): **a1** Through interaction with a substrate; **a2** Through interaction with other nanotubes.

Soon after the first dedicated study of CNT by Iijima et al. [28], collapsed geometries were observed by electron microscopy of large diameter CNT [29]. It is generally admitted now that collapse is favored for large tube diameters and small numbers of concentric tubes [30, 31, 32, 33, 34]. Other collapse parameters at ambient conditions were also identified, including interactions between the external walls of a CNT, interactions with a substrate or with molecular adsorbates [35, 36, 37], defect formation by electron beam irradiation [38], or due to the application of electrostatic fields [39, 40]. The different mechanisms that can be responsible for collapse are illustrated in Figure 1.

For small tube diameters with a stable circular cross-section at ambient conditions, it has been shown that a high external pressure causes collapse. This was first shown for SWCNT, where the collapse pressure has been demonstrated to be a function of CNT diameter [41, 42, 43, 44, 45, 16, 46, 47, 48, 49, 50, 51, 52, 53, 54]. Pressure-induced collapse is also observed for double-wall [55, 56, 57, 58], triple-wall [59] and multi-wall CNT [60]. Any effect of helicity (or chirality) - a geometrical characteristic reported to originate from the configurational tube edge entropy [61] - on the pressure response of CNT was reported to be small, or to occur only in tubes of very small diameters [62].

In this work, we explore the stability conditions of CNT from their circular cross-section to collapsed shapes, focusing on the stability domain as a function of geometrical parameters (diameter and number of tube walls), as well as the effect of external pressure. The instability of the circular cross-section is found to be driven by the competition of the elastic energy, related to the bond-bending energy, and the external and internal forces. External forces include the pressure applied to CNT external surfaces, and interactions with the surrounding molecular medium, while internal forces include the vdW interactions of the tube walls. While a number of atomistic calculations and models have tried to predict the CNT stability conditions [43, 63, 16, 55, 56, 47, 60, 32, 53, 54, 63], none of them fully covered structural tube properties, including tube diameters, number of walls, etc.
In addition, we propose a multiscale approach, showing that the onset of collapse of a range of nanotubes with diameters around a nanometer are well described by the canonical Lévy-Carrier law (LC), formulated 150 years ago [64], and originally developed for the collapse of macroscopic tubes. Our modified LC-based model refered here as the van der Waals-Lévy-Carrier model (vdW-LC) behaves in this domain consistently with atomistic simula-

tions, density-functional tight-binding (DFTB), molecular dynamics (MD), as well as with a macroscale analog based on the deformation of O-rings. Our model is then used to plot collapse phase diagrams for CNT, providing a better understanding of the radial stability and collapse mechanisms of single- and multi-wall nanotubes (SWCNT and MWCNT), including nanotube bundles, as a function of their diameter from the nanometer to dozens of nanometers. We propose, finally, that such an approach could be adapted for more complex porous materials.

2. Results and discussion

2.1. Theoretical SWCNT collapse model

In mechanics, the radial collapse pressure P_c for macroscopic tubes with a diameter d_0, is known to scale as $P_c \propto d_0^{-3}$, as expressed by Lévy-Carrier [64]. At the nanoscale, it has been shown that such a formalism is consistent for SWCNT, when a correction term, $1 - \beta^2/d_0^2$, is included. This term emerges both in simulations, as well in experiments, and may be related to the large built-in curvature energy for small tube diameters, or to the discrete atomistic nature of tube walls [65]. This approach is called the modified LC equation [66], and is written,

$$P_c = \frac{24D}{d_0^3}\left(1 - \frac{\beta^2}{d_0^2}\right), \tag{1}$$

where D is the bending stiffness of graphene, and β corresponds to the diameter of the smallest free-standing stable SWCNT [66] (all parameter values are given in Table 1). When $d_0 \gg \beta$, the LC law is recovered; however, when $d_0 < \beta$, P_c <0, corresponding to unfeasibly small free-standing tube diameters.

Eq.1, originally based on experimental observations and simulations [54], has been shown to be well-suited for SWCNT with diameters in the range $d_0 \sim 0.7$ - 2 nm, and no effects of the tube chirality were seen [66]. With increasingly larger tube diameters, the correction term becomes less important, and the interaction of the external tube with the pressure transmitting medium (PTM) becomes more important. R1.Q1 In order to account for the surrounding PTM (an argon bath in MD simulations), we write the energy per unit of tube length at the collapse pressure as the addition of the elastic

energy, the pressure term and the surface energy γ_{F-C} [32]:

$$E = \frac{12\pi D}{d_0}\left(1-\frac{\beta^2}{3d_0^2}\right) + P_c\frac{\pi}{4}d_0^2 + \gamma_{F-C}\ \pi\ d_0, \quad (2)$$

where the first two terms guarantee that Eq.1 is obtained by minimizing Eq.2 as a function of d_0. With the inclusion of the last term this minimization now leads to:

$$P_c = \frac{24D}{d_0^3}\left(1-\frac{\beta^2}{d_0^2}\right) - 2\frac{\gamma_{F-C}}{d_0}. \quad (3)$$

We will refer below to this expression for the collapse pressure as the already mentioned van der Waals-Lévy-Carrier model, vdW-LC. The applicability of this expression may be affected by the presence of defects which tend to reduce the collapse pressure [67], (not treated in this study).

2.2. Theoretical SWCNT bundle collapse model

For a bundle formed of SWCNT, Eq.3 can be modified following Pugno et al. [68], considering that each individual tube in a bundle interacts with its neighboring tubes, acting as a SWCNT pseudo-fluid, while the outer surface of the bundle interacts with the PTM. Then, P_c can be obtained by minimizing the corresponding enthalpy expression,

$$P_c = \frac{24D}{d_0^3}\left(1-\frac{\beta^2}{d_0^2}\right) - 2\left(\frac{\gamma_{C-C}}{d_0} + \frac{\gamma_{F-C}}{d_B}\right) \quad (4)$$

where d_B represents the bundle diameter. In Eq.4, γ_{C-C} is the carbon-carbon interaction energy, corresponding to the inter-tube vdW interactions, while the last term represents the interaction between the PTM and the external surface of the bundle. It is worth to note that following both Pugno et al. [32], and atomistic modeling [59], the tubes in the bundle will undergo polygonization before collapse. In Eq.4, we made the approximation of circular bundles. The validity of this approximation may affect the pressure collapse determination for bundles made of large tube diameters, more prone to polygonize than ones made of small tubes. However, such an approximation should only affect small bundles, considering that the last term in Eq.4 can be neglected if $d_B \gg 1$. We also may note that total or partial intrusion of the PTM into the interstitial tube space will affect the collapse pressure of bundles. Such an intrusion will indeed prevents polygonalisation and bring

the collapse pressure back towards that of individualized (unbundled) tubes. Such a behavior is outside the scope of this work, and has not been studied here.

2.3. Theoretical MWCNT collapse model

To go a step further, we now generalize our model for MWCNT. We follow the methodology proposed by Gadakar et al. [56] in which friction between tubes is neglected so that the bending stiffnesses are additive. Thus, the net external pressure needed to collapse the N walls of a MWCNT is written as the sum of the pressures P_{c_i} needed to collapse the $i = 1$ to N corresponding individual SWCNT. This is a good approximation provided that the inter-tube separations are small enough that the tubes deform together. Then it does not matter whether the pressure is transmitted to the inner tubes or is entirely supported by the outer tube. To a first approximation, the elastic energy stored in the deformation of the tubes is summed over all the tubes, while the work done by the pressure is due to the reduction in volume of the outer tube. This leads to the additive character of the P_c. Note that this will not be true if the inter-tube distances are large enough to allow the outer tube - or indeed any inner tube - to ovalise significantly while the next smaller tube remains essentially circular [57]. In MWCNT, the vdW inter-wall interactions are compensated, considering that each individual inner-tube interacts both with its next inner- and next outer-tube, i-1 and i+1 respectively. However, it is necessary to account for interaction of the innermost tube (i=0) with only its next larger tube neighbor (i=1), and for the interaction of the outermost tube (i=N-1) with (i=N-2), and finally with the external PTM (the last term in Eq.5). Accounting for all these interactions, the collapse pressure becomes,

$$P_c = \sum_{i=0}^{N-1} \frac{24D}{d_i^3} \left(1 - \frac{\beta^2}{d_i^2}\right) - 2\left(\frac{\gamma_{C-C}}{d_0} - \frac{\gamma_{C-C}}{d_{N-1}} + \frac{\gamma_{F-C}}{d_{N-1}}\right). \quad (5)$$

It is noteworthy that vdW interactions forbid some chirality couples of neighboring tubes i and $i\pm1$, if the latters have close enough chiral angles, as explained elsewhere [69]. For existing MWCNT, inter-tube distances are reported to range in between 0.27 nm and 0.42 nm, however, the most common distances in MWCNT are about 0.32-0.35 nm [70]. For the sake of simplicity, we have considered that all tubes in a MWCNT range at the graphitic interlayer distance δ (see Table.1), and that $d_i = d_0 + 2\delta \cdot i$ in Eq.5. We

Table 1: Parameters used in the various Lévy-Carrier models.

D	1.7 (eV)	Ref [66, 71]
β	0.44 (nm)	Ref [66]
γ_{F-C}	0.11 (J/m^2)	This work
γ_{C-C}	0.23 (J/m^2)	Ref [71, 72, 73]
δ	0.34 (nm)	Ref [71]

may note here that even if a general MWCNT can no longer be considered as a thin tube, our method of evaluation of the collapse pressure as the sum of the contributions of the various thin-walled SWCNT in interaction with their environment permits the use of the LC expression, which is only valid for thin-walled tubes.

2.4. Numerical simulations, experiments and model validation

In order to check the accuracy of our model, we compare it with both numerical and experimental data. Simulations have been performed with two algorithms, DFTB for small tube diameters [74], and MD based on the empirical AIREBO bond order potential [75], accounting both for C-C covalent bonds and for long-range vdW interactions [76]. All MD simulations have been performed for tubes or bundles immersed in an Ar bath at 300K. Ar-Ar and C-Ar interactions were modeled by a (12-6) Lennard-Jones potential, using the Lorentz-Berthelot mixing rule (see section Method for simulation details).

In Fig.2.a, we show the evolution of P_c as a function of the tube diameter from DFTB, MD, and from the theoretical models detailed above. As can be seen, for small d_0, the modified LC approach (bold blue line), is in good agreement with the DFTB simulations (light green stars). When d_0 <0.57 nm, P_c decreases, corresponding to the situation where tube diameters are so small that the curvature energy is large enough to make tubes less stable. In this region, a large deviation is observed below the macroscopic LC law (dashed black line), that does not include the small-diameter correction term discussed above. When d_0 >3nm, the vdW-LC approach (red dotted line) shows another sharp decrease of P_c below the macroscopic LC law, corresponding to tube diameters where interactions between the PTM

and the tube walls dominate over the negligible curvature energy. SWCNT simulations (red circles), show a self-collapse diameter of 5.3 nm, in good agreement with the experimental data reported; about 5.1 nm is cited in the review of He et al. [15]. This agreement then permits the fitting of γ_{F-C} (see Table 1) to the vdW-LC model for SWCNT (Eq.3). As shown in Fig.2.a, we find excellent agreement between simulations and the theoretical model for the full diameter range simulated. We then compare these results with the

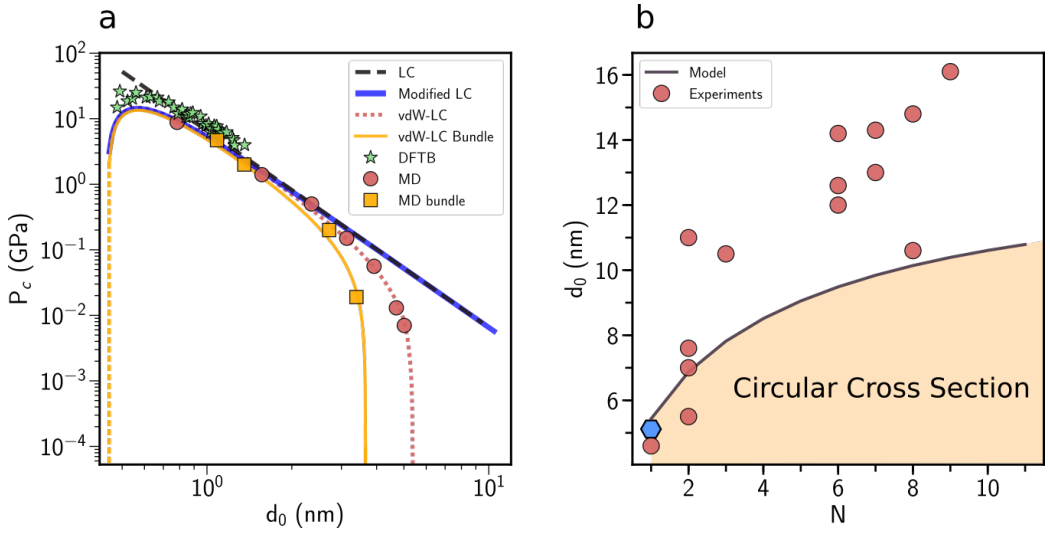

Figure 2: **a.** Collapse pressure P_c of SWCNT as a function of the tube diameter d_0, using three models based on the Lévy-Carrier formula: the standard LC (black dashed line), the modified LC (blue bold straight line) and the vdW-LC models developed in this work for SWCNT (red dotted line), and bundles (yellow line). The results are compared to numerical simulations, DFTB (green stars) and MD simulations with a long-range bond order potentials for SWCNT (red circles), and bundles (yellow squares). **b.** Innermost tube diameters d_0 of MWCNT for which collapsed configurations have been observed experimentally, plotted against the number of tube walls N. The red circles correspond to experimental observation of collapsed tubes, while the blue hexagon corresponds to an averaged experimental measurements of the collapse pressure for SWCNT. The black line corresponds to the prediction from our vdW-LC model. The yellow area corresponds to the phase where tubes are not collapsed (circular cross section), while the part of the diagram above corresponds to nanotubes collapsed at ambient pressure.

vdW-LC model applied to bundles. In Fig.2.a, the yellow squares correspond to the results of simulations performed on bundles containing 37 SWCNT. As can be seen, the self-collapse diameter is smaller than that of isolated

SWCNT, a behavior already observed in [77]. This behavior could be explained by the contribution of tubes polygonization which tends to lower P_c. Using Eq.4 and the γ_{F-C} previously fitted from isolated SWCNT, we see that the vdW-LC model applied to the bundle configuration is in good agreement with simulations using γ_{C-C} (see Table 1). Note that in the bundle used in simulations, $d_B \gg d_0$ and the interaction between the PTM and the external bundle surface could be neglected compared to the inter-tube interactions (Eq.4).

In Fig.2.b, we compare experiment with the vdW-LC for MWCNT (Eq.5). The tube stability is presented as innermost tube diameter d_0 against the number of tube walls N at ambient pressure. The continuous line separating the two domains represents the critical internal diameter for collapse of MWCNT at ambient pressure. The experimental points (red circles) correspond to collapsed tubes observed by electron microscopy, and are extracted from different sources summarized in the work of Balima et al. [34]. As expected, these points are mainly found in the collapsed domain. We have underlined a particular point from the work of He et al. [15] (blue hexagon), which corresponds to the determination of the critical collapse diameter by observations of many SWCNT. This point should then lie on the limiting curve, and is found to be in very good agreement with the prediction of our model. We can also note that two points are found bellow the theoretical prediction. These exceptions may be explained by interactions with the substrate (Fig.1.a1), which are known to favor the tube collapse [78]. Overall, our prediction is consistent with experiments.

The results presented in Fig.2.b also show that with an increasingly higher number of tube walls, MWCNT of larger internal diameter can be stabilized at ambient conditions. Note that the inner-wall vdW interactions may lead to the metastability of a collapsed geometry at a diameter below the critical one [29, 77, 32, 34]. The critical diameter may also be strongly reduced for defective carbon nanotubes [33].

2.5. Nanotube collapse phase diagram

We have demonstrated that the vdW-LC model is a robust, simple and suitable approach in predicting single- and multi-wall carbon nanotubes stability, as well as for bundles. We now use this model to determine the nanotube collapse phase diagram. In Fig.3.a, we plot the stability diagram of MWCNT at ambient pressure, extending beyond the domain explored in Fig.2.b. The stable phase, either circular or collapsed, depends on d_0 and N.

There also exists an instability domain, i.e., in which tubes cannot exist, for very small d_0 (red domain) in Fig.3.a,b. Hence, with an increasingly large d_0, the number of tube walls has to be increased in order to stabilize a circular MWCNT. Nevertheless, d_0 has a maximum at d_0=12nm for N=30 walls, corresponding theoretically to the largest possible internal cavity in MWCNT. For larger N, d_0 slightly decreases and becomes asymptotically constant at d_0=11.3 nm. This behavior results from the competition between the inter-tube vdW and the tube-PTM interactions, corresponding to the second term in the Eq.5.

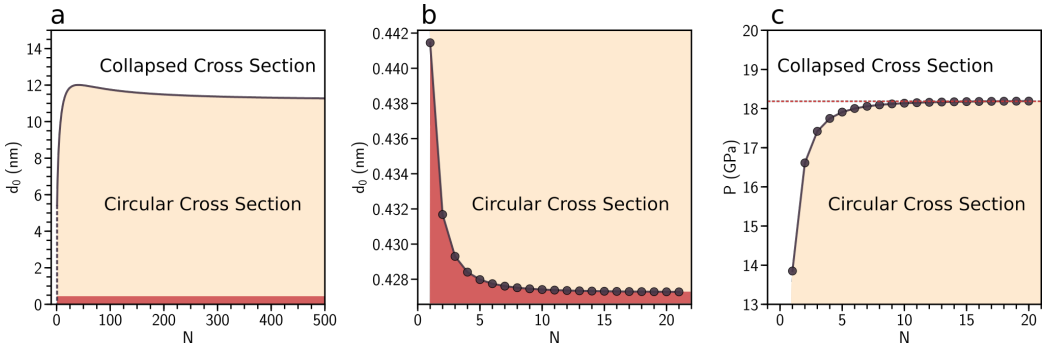

Figure 3: **a**. Stability diagram of carbon nanotubes at ambient pressure as a function of the internal diameter d_0, and the number of tube walls, N. Three regions are defined from the bottom to the top: (1) the red phase corresponds to the tubes that cannot exist due to smaller internal diameter, (2) the yellow phase, corresponding to the stability domain of tubes with a circular cross-section, and (3) the white phase, corresponding to the stability domain of collapsed tubes. **b**. Zoom on the red phase in (a) (unstable tubes), for small tube diameters. **c**. Stability diagram for MWCNT with d_0=0.56 nm, corresponding to the tubes found to show the highest collapse pressure. The red dashed line corresponds to the maximum collapse pressure found in the model.

In Fig.3.b, we see that the smallest possible tube diameter for a free-standing SWCNT corresponding to d_0=0.44 nm [66] can be slightly reduced when increasing the number of tube walls. This result is qualitatively supported in the literature, where d_0 ∼0.407nm has been reported for double-wall carbon nanotubes [79], and d_0 ∼0.3nm for a N=13 MWCNT [80]. Our calculations do not allow for internal tube diameters below ∼0.43nm. Such a limitation could results from the tube-substrate interactions, the discrete distribution of carbon atoms in the wall, or the small tube diameter helicities, neglected

in the model, and going beyond the scope of this work.

The maximum pressure needed to collapse any MWCNT can now be found by searching the maximum collapse pressure from Eq.5, as a function of d_0 and N. The maximum P_c value depends on N but is found invariably at d_0 ∼0.56 nm whatever the value of N. The maximum value of P_c evolves from P_c ∼13.9 GPa for SWCNT and progressively increases with N, converging to a maximum at P_c=18.2 GPa. As shown in Fig.3.c, we note the quick convergence of P_c for N ranging from 1 to 4. The number of walls is thus found to increase the stability pressure by about ∼30%, corresponding to the observations on deformed or collapsed geometries for MWCNT with a relatively high number of walls in nanocomposites under compression [34]. We now use the model to find how P_c evolves as a function of d_0, for N ranging from 1 to 100, in the collapse phase diagram, Fig.4.a. As can be seen, for small d_0, N has no significant effect on P_c. So, we may approximate that all curves collapse in a single one for internal diameters below d_0 ∼1nm. For larger d_0, N plays a more significant role on tubes stability. Interestingly, in Fig.4.b, the collapse pressures obtained with the LC model are comparable with those from the vdW-LC model for certain tubes. We consider a multiscale domain when the $P_c d_0^3$ plotted as function of d_0 can be approximated by the LC law corresponding to a constant. We show this behavior for N = 1, 2, 3, 5, 10, 20 and 100, where the continuous part of plots can be assimilated to horizontal lines, assuming an uncertainty on experimental pressure determinations of the order of ±5 %. In Fig 4.c, we show the tube diameter as a function of the number of walls into the multiscale domain. We thus observe that SWCNT with diameters ranging from 0.95 to 2.5 nm behave as macroscopic tubes. This diameter domain is shifted as a function of N to higher diameters, and converging for N = 20, for internal diameters ranging from ∼3.5 to ∼7.5 nm. The chosen accuracy of ±5 % corresponds to a conservative choice of pressure determination in high-pressure measurements [81]. This link between the nano- and the macroscopic scales can be understood from the dominant role played by the innermost tube on pressure stability, as shown in Fig. 3.a. It is noteworthy that such a multiscale behavior has been previously reported in the case of SWCNT [43, 82]. We may discuss aspects which could limit the validity of the proposed model and the phase diagrams derived from it. As already pointed out, the parameters in Eq. 3 may be affected by the density of defects which will tend to reduce the collapse pressure [67]. We have also made the hypothesis of a uniform inter-wall distance in MWCNT, which is not always valid [83]. This effect is

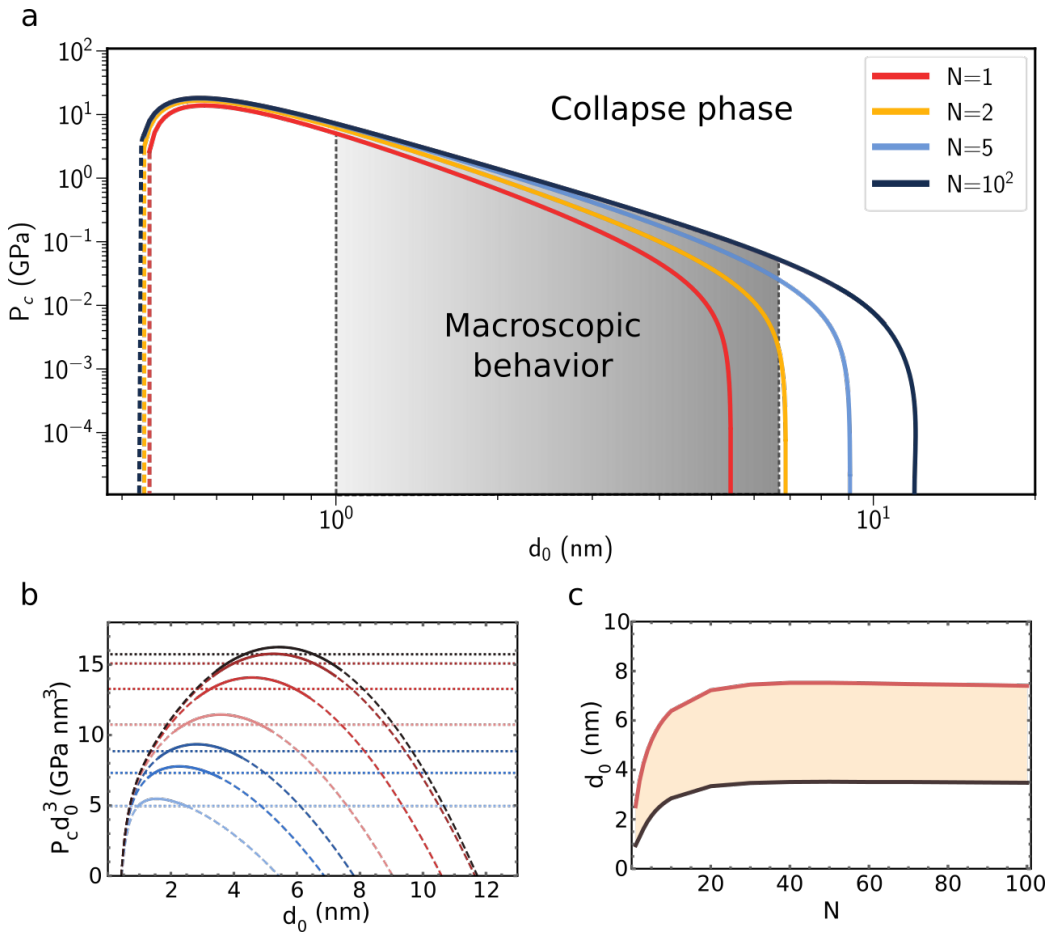

Figure 4: **a.** Collapse pressure P_c as a function of the innermost tube diameter d_0 for different numbers of tube walls N, ranging from 1 to 100 and determined from the theoretical model accounting for vdW interactions. The gray area represents the multiscale domain, i.e. a d_0 range where the original macroscopic LC model agrees with the vdW-LC model at the nanoscale (see text and (b) for details and criteria). **b.** Normalized collapse pressure $P_c d_0^3$ as function of the internal diameter for tubes with N=1, 2, 3, 5, 10, 20 and 100 walls from inner to outer curves. The continuous part of the curves represent the domain in which within ± 5 % accuracy, a macroscopic LC model (horizontal dashed lines) can be used to approximate the vdW-LC one. **c.** Domain of validity of the continuum mechanics corresponding to the LC model (yellow area). We have considered that the LC model is valid when it differs by less than 5% from a linear approximation in the $P_c d_0^3$ representation as function of d_0.

indeed difficult to take into account in the model as developed. We need also to consider if other transformations may take place before the collapse transition, in particular the possibility of pressure induced sp^3 interlink between tubes, or the evolution towards the diamond structure or other mixed sp^2-sp^3 structures [84], as well as other carbon sp^3 structures [85]. Experiments show that for SWCNT tube bundles with diameters of 1.35 nm, diamond formation takes place subsequently to the collapse pressure [86], favoured by the combination of high pressure and high temperature conditions. This will be the most common scenario, but we may wonder if it also prevails for the most stable tubes, i.e., tubes with an internal diameter around 0.56 nm. For such tubes, depending on the number of tube walls, our model predicts a collapse pressure ranging from 13.9 to 18 GPa. Tube interlinking or polymerization has already been proposed from atomistic modeling [87, 88], which is particularly favored by low diameter tubes. To the best of our knowledge, no experimental results have yet shown the formation of such mixed sp^2-sp^3 structures. Calculations also show that even after pressure-induced interlinking is produced, the transformation can be totally reversible [89].

3. A macroscopic model for the collapse of carbon nanotubes

We have shown above that Eq.1 is a suitable multiscale equation for comparing the collapse behavior of macroscopic tubes with certain tubes at the nanoscale. This result is thus consistent in predicting P_c for SWCNT with diameters ranging from $d_0 \sim$ 1-2 nm and for MWCNT with a limited number of tube walls. Note that the diameter range reported corresponds to the most common tube diameters produced experimentally [90]. In order to verify this theoretical result, we have developed a table-top experiment using macroscopic nitrile rubber rings to mimic CNT. In this experiment, nanotubes are replaced by macroscopic toroidal rings (O-rings) with the diameters d_0=11.25, 13.7, 16.25 and 28.75 mm. The O-rings are placed between two transparent plates to limit movement in the direction of the torus axis. A pressure vessel is made by using a large outer O-ring surrounding the smaller inner one. The vessel is connected to a bicycle pump with a pressure gauge to generate and monitor the pressure acting on the inner O-ring (Fig.5.a). The deformation of this O-ring is measured as a function of the applied pressure, and quantifieded by image analysis (details are given in the section Method). The O-rings used in this experiment are not strictly speaking tubes, but rings, and we first verify that they follow the LC law.

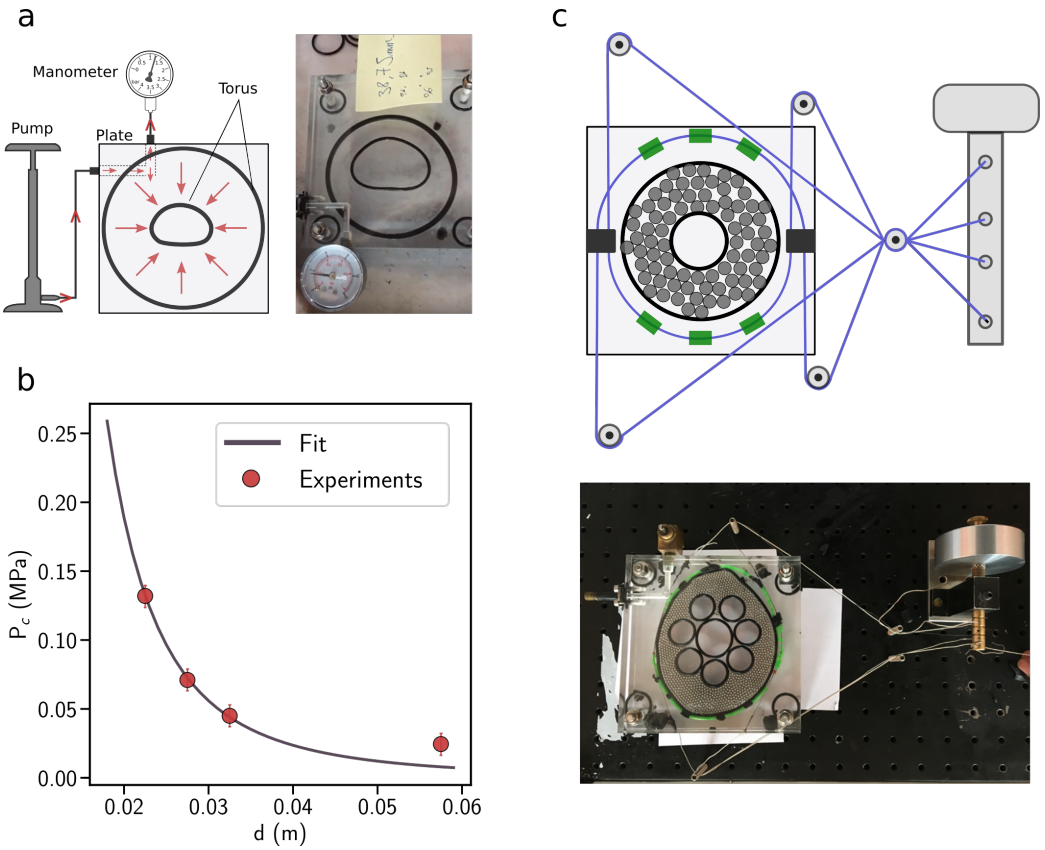

Figure 5: **a.** Schema and picture of the experiment, in which O-rings are collapsed by a fluid pressure medium (air or water). **b.** Averaged collapse pressure P_c of O-rings in the experiment described in (a), as a function of their diameters d (red circles). Experimental data are found to fit $P_c \propto d^{-3.0\pm0.7}$ (black line). **c.** Schema and picture of the experiment in which O-rings are collapsed by a solid pressure medium (ball-bearings).

To do so, four measurements per O-ring diameters have been performed, and the averaged data are shown in Fig.5.b. The data are fitted by an inverse power law, $P_c = a.D^{-\alpha}$ with a=1.51 J (a constant), and α=3.0 $\pm$ 0.7, as expected from Eq.1. The O-rings are thus demonstrated to have a similar radial mechanical response to macroscopic tubes, and can reasonably be used for comparison with SWCNT with d_0 ranging from $\sim$1 to 3.45 nm.

In Fig.6, we compare the dynamical collapse behavior of a macroscopic O-ring bundle with data from MD simulations at the nanoscale. In the experiment, a bundle of 37 O-rings is surrounded by a bath of steel ball-bearings acting as a PTM. Pressure is applied by tightening a sheathed guitar string surrounding the ball-bearings (Fig.5.c). The change of PTM (ball-bearings

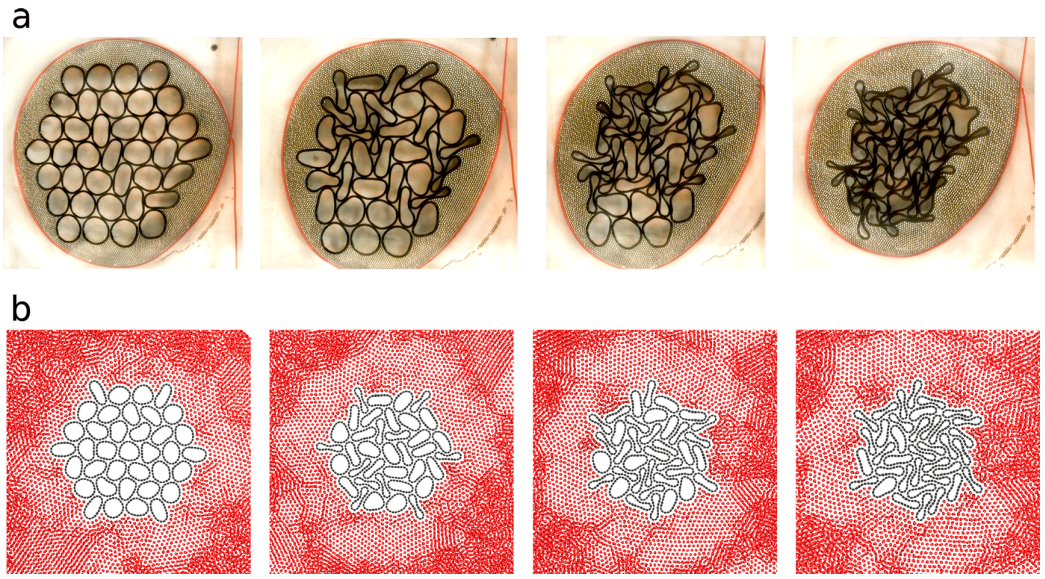

Figure 6: **a.** Evolution of a 37 O-ring bundle immersed in a ball-bearing pressure-transmitting medium during a compression cycle. **b.** Collapse behavior of a 37 SWCNT bundle immersed in a solid argon medium. Simulation was performed at pressures ranging from 1 to 3 GPa with a pressure increased from the left to the right.

instead of air or water) compared to the previous experiment (Fig.5.a) is necessary to match simulations. Indeed, the pressure needed to collapse a bundle with SWCNT diameter around 1 nm is a few GPa, a pressure at which the argon PTM used in simulation and in experiment is solid [91]. The ball-bearings tend to form an hexagonal close-packed planar domain, which mimic a macro-crystalline argon PTM. In the simulation, we have

built a bundle formed of 37 SWCNT with d_0=1.3nm, immersed in an argon bath at P ∼2GPa. Collapse experiments on O-rings are compared to these MD simulations in Fig.6. The collapse process in both cases is found to be in good qualitative agreement. In the early stages, tubes show a small deformation. Then some of the tubes collapse to a peanut shape, while others stay circular or ovalize. Later in the semi-collapsed state, a large number of tubes have collapsed, but a few tubes remain ovalized. At the end of the process, all tubes show a collapsed shape. Note that both experiments and simulations show that in a solid PTM, the collapse of a SWCNT bundle, at least when it can be assimilated to a macroscopic bundle, is a complex and non-homogeneous process. It has already been shown that collapse of even a single isolated elastic ring is not instantaneous [92] - complete at P_c - but goes progressively through ovalisation to collapse shape over the range P_c to $1.5P_c$, see also Fig.3 in [54].

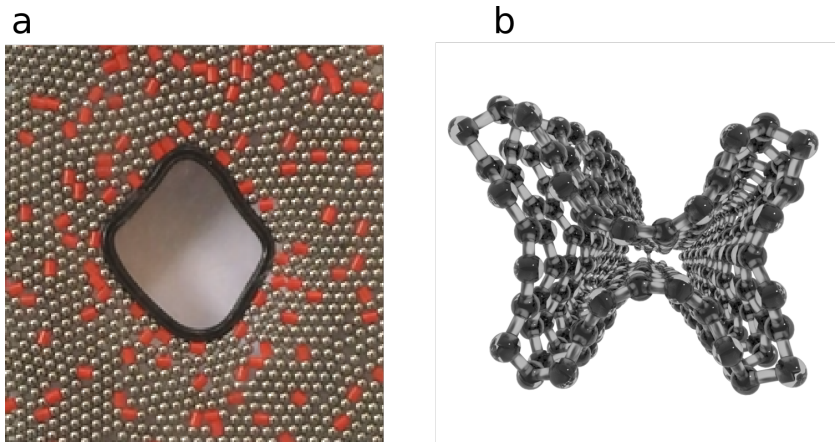

Figure 7: **a.** Four-lobe collapse of an O-ring obtained using a mixed medium of ball bearings and plastic beads (red colour). The mixed medium leads to the formation of smaller crystalline domains in the pressurized transmitting medium. **b.** Numerical simulation of tube collapse with a metastable state corresponding to a four-lobe shape (the pressure transmitting medium is not shown in this snapshot).

Our table-top set-up allows for multiple variations to study specific effects. For instance, we noticed that using the scheme of Fig. 5.c with individual O-rings, the polycrystalline organization of the ball bearings set up a stable structure which prevented the collapse of the tube. Instead, the PTM grain structure induced irregularities at the surface of the O-ring. Fig.7.a, shows

the possibility of reducing the PTM grain-size using a mixed medium by disseminating other types of particles, plastic beads, into the ball bearing PTM. Despite this trick, we were not able to totally collapse this O-ring due to the remaining grain domains and the limitations in the applied pressure in the set-up. Nevertheless, we could observe an incipient 4-lobe collapse, a metastable configuration which also appeared in some of our MD simulations. R2.Q7 We show in Fig.7.b a metastable four-lobe shape obtained by MD simulations. In simulations, such a geometry was found to evolve from four lobes to three, then to a stable collapse shape as a function of time.

4. Conclusion

We propose a simple theoretical model to determine the stability domain of carbon nanotubes as a function of their diameters and their number of walls. The geometrical stability limits at ambient pressure, as well as collapse pressures for arbitrary number of walls, are characterized from the long-range van der Waals interactions, introduced into the modified Lévy-Carrier equation, formulated for tubes at the nanoscale. The model proposed in this work is validated by numerical simulations at the nanoscale, as well as experiments at the macroscale. We have thus found that depending on the number of tube walls, nanotubes show a maximum collapse pressure of $\sim$18 GPa with an inner-tube diameter of d_0=12nm. It is noteworthy that our model fits experimental data despite neglecting multi-wall nanotubes inter-layer friction. When d_0 is smaller than 0.56nm, the collapse pressure drops right down, due to the strong tube curvature, resulting in unstable nanotubes. For large tube diameters, the collapse pressure decreases, corresponding to the van der Waals interactions that tend to favor the collapse. From the collapse phase diagrams plotted with the model presented in this work, we have shown that the Lévy-Carrier equation (originally established for macroscopic tubes) is compatible with intermediate tube diameters, one to a few nanometers, and depending on the number of tube walls. This is an important result underlying that the collapse process of most of the common nanotubes produced by standard experimental techniques takes place as in macroscopic tubes, linking behavior at the nanoscale to the macroscale. This behavior was verified by comparing numerical simulations with experiments at the nanoscale and at the macroscale, where nanotubes were replaced by polymer O-rings. We think that such an analogy may be interesting in the study of the mechanical deformation of nanotubes under pressure, as well as in the study of more

complex porous systems as Metal Organic Frameworks (MOF), zeolites, or even disordered porous materials as kerogen.

5. Methods

5.1. Numerical simulations

Density functional tight-binding calculations were performed using the DFTB software package [74] with the matsci-0-3 parameter [93]. Since carbon nanotubes are relatively inert structures where no significant charge transfer is expected [94], we decided to adopt the non-self-consistent charge scheme of DFTB [93]. This algorithm was used only for small tube diameters ranging from d_0=0.5 to 1.4nm, due to the computational time. In this approach, the Kohn-Sham density-functional theory is approximated with fitted integrals from reference calculations. The method increases simulations efficiency compared to density functional theory (DFT), while keeping "a priori" a better accuracy compared to the empirical approaches. The C-C Slater-Koster parameters implemented in this work have been extensively used for CNT simulations and can be found elsewhere [93]. In Fig.2.a, we have determined P_c for a dozen armchair SWCNT. For each pressure, a random displacement of 0.002nm is applied on each atom, and both atomic positions and cell vectors were optimized until the magnitude of all forces became smaller than 10^{-4} Ha/Bohr. In this process, P was increased by steps of 0.2 GPa, up to the tube collapse. This phenomenon is generally found to be abrupt, and can be easily identified from a discontinuity in the enthalpy as a function of P, corresponding to the transformation in a collapse shape. In some rare cases, especially for small d_0, the discontinuity is not visible, and P_c was determined by eye, i.e., we assigned P_c to the first collapsed geometry found.

A second set of simulations using an MD algorithm were performed to study larger tube diameters. MD simulations were conducted for systems with SWCNT immersed in an argon bath, in order to transmit pressure to the nanotubes. Inter-atomic interactions (Ar-Ar and Ar-C) were modelled by a (12-6) Lennard-Jones potential (LJ), with a cutoff fixed at 2 nm,

$$U = 4\,\epsilon\left[\left(\frac{\sigma}{r}\right)^{12} - \left(\frac{\sigma}{r}\right)^{6}\right], \tag{6}$$

Table 2: Lennard-Jones parameters for argon and carbon atoms.

Atoms	σ (nm)	ϵ (meV)
Ar-Ar	0.341	10.3
C-C	0.336	2.4
Ar-C	3.382	5

where σ corresponds to the atomic diameter, r_{ij} is the inter-atomic distance, and ϵ_{ij} is the interaction energy between two atoms i and j. The LJ parameters (given in Table 2) for the interactions of the different species are determined with the Lorentz-Berthelot mixing rule as,

$$\sigma_{ij} = \left(\frac{\sigma_i \ + \ \sigma_j}{2}\right) \qquad \text{and} \qquad \epsilon_{ij} = \sqrt{\epsilon_i \epsilon_j}, \tag{7}$$

The C-C interactions were modelled with the long range bond order potential AIREBO [75]. This potential models both carbon covalent bonds, and long range vdW interactions with a cutoff fixed at 2 nm.

The first step of simulations consists in adsorbing Ar molecules in a bulk phase with the grand canonical Monte Carlo algorithm GCMC (μ_{Ar},V,T), where μ_{Ar} is the chemical potential of Ar, V the volume of the simulation box at T=300K. GCMC was thus performed to generate a pure argon bulk configuration at pressures of about P=2 GPa. A tube (or a bundle) is then inserted inside the bulk configuration, and the inner part of the tube is cleared of argon atoms. MD simulations are then performed with the molecular dynamic LAMMPS package (March 2018 version) [95] on 96 CPU in the isothermal-isobaric ensemble (N,P,T), for a total time of 5 ns, with a time step fixed at 1 fs. P_c is thus determined from the enthalpy as a function of P. When tube collapse occurs, the tube energy changes abruptly, and the collapse pressure can be easily identify. Depending on the PTM, the collapse event can occurs quickly (less than 1 ns) or more slowly, especially near the collapse line shown above in the collapse phase diagrams. It is noteworthy that in this particular area of the diagrams, some transitions from circular to collapsed shapes may be missed due to the slow collapse kinetics, and the limited calculation time that is feasible with the MD algorithm.) In Fig.8, we show the evolution of the shape of a SWCNT with d_0 $\sim$5 nm at P$\sim$0.5 MPa.

As can be seen, the tube goes from a circular to a collapsed shape, corresponding to its equilibrium state in these thermodynamic conditions. For all simulations performed in this work, we used zigzag SWCNT.

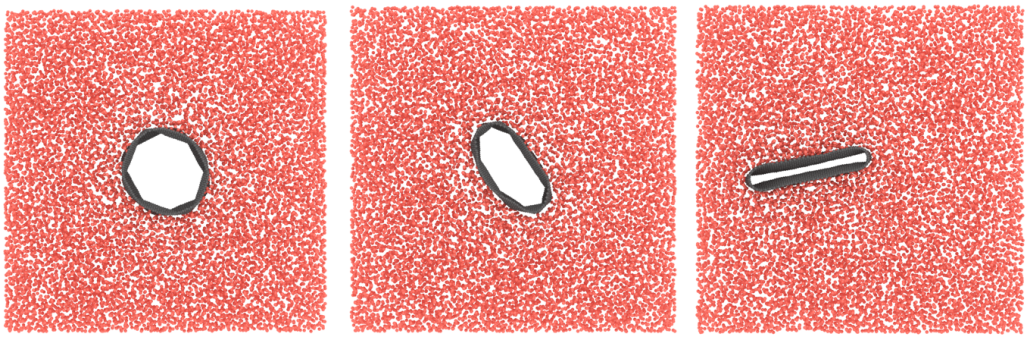

Figure 8: Shape evolution of a SWCNT with d_0 ∼5 nm immersed into an argon bath at a pressure of P∼0.5 MPa. The two first snapshots correspond to out of equilibrium configurations. The last configuration corresponds to an equilibrium state in a collapse shape.

5.2. Experiments

In order to mimic the elastic properties of the radial buckling of SWCNT, we have used toroidal elastomer gaskets (O-rings), usually used for applications such as vacuum seals. O-rings were placed between two transparent plates of PMMA (poly(methyl methacrylate)) with 25mm thickness, while a larger gasket diameter was used to create a cavity around the smaller one. We then used dynamometric keys in order to ensure a uniform small pressure on the O-rings. Both O-rings and internal plate surfaces were oiled in order to reduce the friction. Holes drilled into the top plate were used to connect a bicycle pump and a manometer to vary and monitor the pressure, Fig.9. A schema and a picture of the experiment is shown in Fig.5.a. Doing so, we were able to observe the effect of a radially applied pressure on O-rings for different diameters (d_0=11.25, 13.7, 16.25 and 28.75 mm), with displacements constrained in the plane. In order to validate using O-rings in imitation of SWCNT in the consistent LC domain, we have first shown that they conform to the macroscopic LC approach itself, i.e., that the collapse pressure is inversely proportional to the cube of the torus diameter, Fig.5.b.

The second experiment conducted in this work investigates the deformation of O-rings using a pressure-transmitting medium that mimics the situation

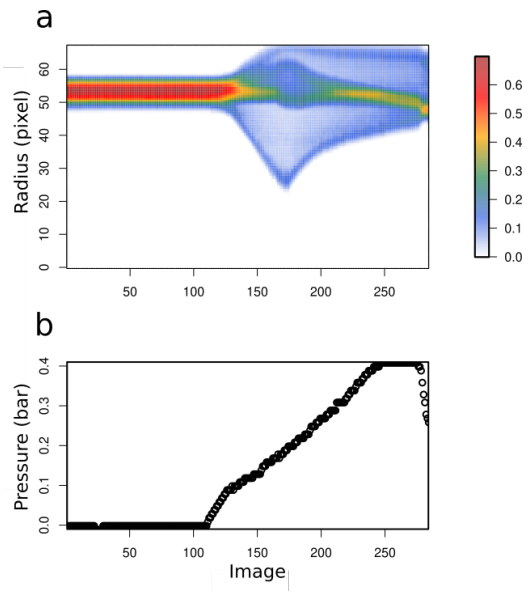

Figure 9: Determination of the collapse pressure for individual O-rings from video image analysis during the compression following the scheme of Fig.5.a. **a.** Time evolution of O-ring radial sectors, measured in pixels from the image. The color scale represents the radial distribution of the pixels detected. The higher this value, the more the O-ring presents a circular shape. On the contrary, the lower this value, the more the O-ring deviates from a circular shape, corresponding to collapse. **b.** Pressure measured from the manometer in image analysis. The correlation with (a) allows the determination of the collapse pressure.

where SWCNT are immersed in a high-pressure (>1GPa) argon PTM. To do this, we have used 2.38 mm steel balls (ball bearings) enclosed by a guitar string sheathed in a plastic tube with nearly the same diameter as the balls, applying pressure on the O-ring surfaces. The steel balls tend to form crystalline grains around the O-rings. The use of plastic beads with similar dimensions to the steel balls allowed modification of the grain size. The application of pressure cycles or the introduction of a vibrating platform would be alternative methods (not tried) to have better control of the PTM grain size.

Acknowledgments

We acknowledge the platform PLECE of the University de Lyon and iLMTech (CNRS and University Claude Bernard Lyon 1). Y. Magnin gratefully acknowledges the Computational Center of Cergy-Pontoise University (UCP) for the computational time. A. San-Miguel and D. J. Dunstan acknowledge the support of the 2D-PRESTO ANR-19-CE00-0027 project. All authors thanks C. Bailly for her help in photo-shopping experimental photography.

References

[1] H. W. Kroto, J. R. Heath, S. C. O'Brien, R. F. Curl, R. E. Smalley, C60: Buckminsterfullerene, nature 318 (6042) (1985) 162–163.

[2] A. K. Geim, K. S. Novoselov, The rise of graphene, in: Nanoscience and technology: a collection of reviews from nature journals, World Scientific, 2010, pp. 11–19.

[3] S. Iijima, T. Ichihashi, Single-shell carbon nanotubes of 1-nm diameter, nature 363 (6430) (1993) 603–605.

[4] N. Yang, G. Zhang, B. Li, Carbon nanocone: A promising thermal rectifier, Applied Physics Letters 93 (24) (2008) 243111.

[5] D. Wei, Y. Liu, The intramolecular junctions of carbon nanotubes, Advanced materials 20 (15) (2008) 2815–2841.

[6] S. Nasir, M. Z. Hussein, Z. Zainal, N. A. Yusof, Carbon-based nanomaterials/allotropes: A glimpse of their synthesis, properties and some applications, Materials 11 (2) (2018) 295.

[7] T. C. Dinadayalane, J. Leszczynski, Fundamental structural, electronic, and chemical properties of carbon nanostructures: graphene, fullerenes, carbon nanotubes, and their derivatives, Handbook of computational chemistry (2012) 793–867.

[8] L.-M. Peng, Z. Zhang, S. Wang, Carbon nanotube electronics: recent advances, Materials today 17 (9) (2014) 433–442.

[9] M. M. Shulaker, G. Hills, N. Patil, H. Wei, H.-Y. Chen, H.-S. P. Wong, et al., Carbon nanotube computer, Nature 501 (7468) (2013) 526–530.

[10] K. Chen, W. Gao, S. Emaminejad, D. Kiriya, H. Ota, H. Y. Y. Nyein, et al., Printed carbon nanotube electronics and sensor systems, Advanced Materials 28 (22) (2016) 4397–4414.

[11] E. Halakoo, A. Khademi, M. Ghasemi, M. Yusof, R. J. Gohari, A. F. Ismail, Production of sustainable energy by carbon nanotube/platinum catalyst in microbial fuel cell, Procedia CIRP 26 (2015) 473–476.

[12] H. Kim, K.-Y. Park, J. Hong, K. Kang, All-graphene-battery: bridging the gap between supercapacitors and lithium ion batteries, Scientific reports 4 (2014) 5278.

[13] T. Saito, T. Yamada, D. Fabris, H. Kitsuki, P. Wilhite, M. Suzuki, et al., Improved contact for thermal and electrical transport in carbon nanofiber interconnects, Applied Physics Letters 93 (10) (2008) 102108.

[14] A. Bianco, K. Kostarelos, M. Prato, Applications of carbon nanotubes in drug delivery, Current opinion in chemical biology 9 (6) (2005) 674–679.

[15] M. He, J. Dong, H. Wang, H. Xue, Q. Wu, B. Xin, et al., Advance in close-edged graphene nanoribbon: Property investigation and structure fabrication, Small 15 (29) (2019) 1804473. doi:10.1002/smll.201804473.

[16] P. Tangney, R. B. Capaz, C. D. Spataru, M. L. Cohen, S. G. Louie, Structural transformations of carbon nanotubes under hydrostatic pressure, Nano Lett. 5 (11) (2005) 2268–2273. doi:10.1021/nl051637p.

[17] S. Rols, I. N. Goncharenko, R. Almairac, J. L. Sauvajol, I. Mirebeau, Polygonization of single-wall carbon nanotube bundles under high pressure, Phys. Rev. B 64 (2001) 153401. doi:10.1103/PhysRevB.64.153401.

[18] P. E. Lammert, P. Zhang, V. H. Crespi, Gapping by squashing: Metal-insulator and insulator-metal transitions in collapsed carbon nanotubes, Phys. Rev. Lett. 84 (2000) 2453–2456.

[19] M. S. C. Mazzoni, H. Chacham, Bandgap closure of a flattened semiconductor carbon nanotube: A first-principles study, Applied Physics Letters 76 (12) (2000) 1561–1563.

[20] L. Yang, J. Han, Electronic structure of deformed carbon nanotubes, Phys. Rev. Lett. 85 (2000) 154–157.

[21] O. Gülseren, T. Yildirim, S. Ciraci, Ç. Kılıç, Reversible band-gap engineering in carbon nanotubes by radial deformation, Physical Review B 65 (15) (2002) 155410.

[22] A. Impellizzeri, P. Briddon, C. P. Ewels, Stacking- and chirality-dependent collapse of single-walled carbon nanotubes: A large-scale density-functional study, Phys. Rev. B 100 (2019) 115410.

[23] C. E. Giusca, Y. Tison, S. R. P. Silva, Atomic and electronic structure in collapsed carbon nanotubes evidenced by scanning tunneling microscopy, Physical Review B 76 (3) (2007) 035429.

[24] F. Balima, S. Le Floch, C. Adessi, T. F. Cerqueira, N. Blanchard, R. Arenal, et al., Radial collapse of carbon nanotubes for conductivity optimized polymer composites, Carbon 106 (2016) 64–73.

[25] L. Duclaux, Review of the doping of carbon nanotubes (multiwalled and single-walled), Carbon 40 (10) (2002) 1751 – 1764, carbon Nanotubes:The Present State.

[26] X. Ma, L. Adamska, H. Yamaguchi, S. E. Yalcin, S. Tretiak, S. K. Doorn, et al., Electronic structure and chemical nature of oxygen dopant states in carbon nanotubes, ACS nano 8 (10) (2014) 10782–10789.

[27] D. Machon, V. Pischedda, S. Le Floch, A. San-Miguel, Perspective: High pressure transformations in nanomaterials and opportunities in material design, Journal of Applied Physics 124 (16) (2018) 160902.

[28] S. Iijima, Helical microtubules of graphitic carbon, Nature 354 (6348) (1991) 56–58.

[29] N. G. Chopra, L. X. Benedict, V. H. Crespi, M. L. Cohen, S. G. Louie, A. Zettl, Fully collapsed carbon nanotubes, Nature 377 (6545) (1995) 135–138.

[30] L. X. Benedict, N. G. Chopra, M. L. Cohen, A. Zettl, S. G. Louie, V. H. Crespi, Microscopic determination of the interlayer binding energy in graphite, Chemical Physics Letters 286 (5) (1998) 490 – 496.

[31] T. Tang, A. Jagota, C.-Y. Hui, N. J. Glassmaker, Collapse of single-walled carbon nanotubes, J. Appl. Phys. 97 (7) (2005) –. doi:10.1063/1.1883302.

[32] N. M. Pugno, The design of self-collapsed super-strong nanotube bundles, J. Mech. Phys. Solids 58 (9) (2010) 1397–1410.

doi:10.1016/j.jmps.2010.05.007.
URL http://www.sciencedirect.com/science/article/pii/S0022509610000979

[33] C. Zhang, K. Bets, S. S. Lee, Z. Sun, F. Mirri, V. L. Colvin, et al., Closed-edged graphene nanoribbons from large-diameter collapsed nanotubes, ACS Nano 6 (7) (2012) 6023–6032.

[34] F. Balima, S. L. Floch, C. Adessi, T. F. Cerqueira, N. Blanchard, R. Arenal, et al., Radial collapse of carbon nanotubes for conductivity optimized polymer composites, Carbon 106 (2016) 64 – 73.

[35] T. Hertel, R. E. Walkup, P. Avouris, Deformation of carbon nanotubes by surface van der waals forces, Phys. Rev. B 58 (1998) 13870–13873.

[36] K. Yan, Q. Xue, Q. Zheng, D. Xia, H. Chen, J. Xie, Radial collapse of single-walled carbon nanotubes induced by the cu2o surface, J. Phys. Chem. C 113 (8) (2009) 3120–3126. arXiv:http://pubs.acs.org/doi/pdf/10.1021/jp808264d, doi:10.1021/jp808264d.

[37] J. Xie, Q. Xue, H. Chen, D. Xia, C. Lv, M. Ma, Influence of solid surface and functional group on the collapse of carbon nanotubes, The Journal of Physical Chemistry C 114 (5) (2010) 2100–2107.

[38] N. G. Chopra, F. Ross, A. Zettl, Collapsing carbon nanotubes with an electron beam, Chemical Physics Letters 256 (3) (1996) 241 – 245.

[39] O. E. Shklyaev, E. Mockensturm, V. H. Crespi, Modeling electrostatically induced collapse transitions in carbon nanotubes, Phys. Rev. Lett. 106 (2011) 155501.

[40] H. R. Barzegar, A. Yan, S. Coh, E. Gracia-Espino, G. Dunn, T. Wågberg, et al., Electrostatically driven nanoballoon actuator, Nano Letters 16 (11) (2016) 6787–6791.

[41] A. Sood, P. Teresdesai, D. Muthu, R. Sen, A. Govindaraj, C. Rao, Pressure behaviour of single wall carbon nanotube bundles and fullerenes: A raman study, Phys. Status Solidi B 215 (1) (1999) 393–401, International Conference on Solid State Spectroscopy - (ICSSS), Schwabisch Gmund, Germany, Sep 05-07, 1999. doi:{10.1002/(SICI)1521-3951(199909)215:1<393::AID-PSSB393>3.0.CO;2-8}.

[42] S.-P. Chan, W.-L. Yim, X. G. Gong, Z.-F. Liu, Carbon nanotube bundles under high pressure: transformation to low-symmetry structures, Phys. Rev. B 68 (2003) 075404. doi:10.1103/PhysRevB.68.075404.

[43] R. B. Capaz, C. D. Spataru, P. Tangney, M. L. Cohen, S. G. Louie, Hydrostatic pressure effects on the structural and electronic properties of carbon nanotubes, Phys. Status Solidi B 241 (14) (2004) 3352–3359. doi:10.1002/pssb.200490021.

[44] J. A. Elliott, J. K. W. Sandler, A. H. Windle, R. J. Young, M. S. P. Shaffer, Collapse of single-wall carbon nanotubes is diameter dependent, Phys. Rev. Lett. 92 (2004) 095501. doi:10.1103/PhysRevLett.92.095501.

[45] A. Merlen, N. Bendiab, P. Toulemonde, A. Aouizerat, A. San Miguel, J. L. Sauvajol, et al., Resonant raman spectroscopy of single-wall carbon nanotubes under pressure, Phys. Rev. B 72 (2005) 035409. doi:10.1103/PhysRevB.72.035409.

[46] S. Zhang, R. Khare, T. Belytschko, K. J. Hsia, S. L. Mielke, G. C. Schatz, Transition states and minimum energy pathways for the collapse of carbon nanotubes, Phys. Rev. B 73 (2006) 075423. doi:https://doi.org/10.1103/PhysRevB.73.075423.

[47] M. Hasegawa, K. Nishidate, Radial deformation and stability of single-wall carbon nanotubes under hydrostatic pressure, Phys. Rev. B 74 (2006) 115401.

[48] C. Caillier, D. Machon, A. San-Miguel, R. Arenal, G. Montagnac, H. Cardon, et al., Probing high-pressure properties of single-wall carbon nanotubes through fullerene encapsulation, Phys. Rev. B 77 (12) (2008) 125418.

[49] M. Yao, Z. Wang, B. Liu, Y. Zou, S. Yu, W. Lin, et al., Raman signature to identify the structural transition of single-wall carbon nanotubes under high pressure, Phys. Rev. B 78 (20) (2008) 205411. doi:10.1103/PhysRevB.78.205411.

[50] A. J. Ghandour, D. J. Dunstan, A. Sapelkin, G-mode behaviour of closed ended single wall carbon nanotubes under pressure, physica status solidi (b) 246 (3) (2009) 491–495.

[51] C. A. Kuntscher, A. Abouelsayed, K. Thirunavukkuarasu, F. Hennrich, Pressure-induced phenomena in single-walled carbon nanotubes: Structural phase transitions and the role of pressure transmitting medium, physica status solidi (b) 247 (11-12) (2010) 2789–2792.

[52] Y. Sun, D. Dunstan, M. Hartmann, D. Holec, Nanomechanics of carbon nanotubes, PAMM 13 (1) (2013) 7–10.

[53] T. F. Cerqueira, S. Botti, A. San-Miguel, M. A. Marques, Density-functional tight-binding study of the collapse of carbon nanotubes under hydrostatic pressure, Carbon 69 (0) (2014) 355–360. doi:10.1016/j.carbon.2013.12.036.

[54] A. C. Torres-Dias, T. F. Cerqueira, W. Cui, M. A. Marques, S. Botti, D. Machon, et al., From mesoscale to nanoscale mechanics in single-wall carbon nanotubes, Carbon 123 (2017) 145 – 150. doi:http://dx.doi.org/10.1016/j.carbon.2017.07.036.

[55] X. Ye, D. Y. Sun, X. G. Gong, Pressure-induced structural transition of double-walled carbon nanotubes, Phys. Rev. B 72 (2005) 035454. doi:10.1103/PhysRevB.72.035454.
URL http://link.aps.org/doi/10.1103/PhysRevB.72.035454

[56] V. Gadagkar, P. K. Maiti, Y. Lansac, A. Jagota, A. K. Sood, Collapse of double-walled carbon nanotube bundles under hydrostatic pressure, Phys. Rev. B 73 (2006) 085402. doi:10.1103/PhysRevB.73.085402.

[57] A. L. Aguiar, E. B. Barros, R. B. Capaz, A. G. Souza Filho, P. T. C. Freire, J. Mendes Filho, et al., Pressure-induced collapse in double-walled carbon nanotubes: Chemical and mechanical screening effects, J. Phys. Chem. C 115 (13) (2011) 5378–5384.

[58] S. You, M. Mases, I. Dobryden, A. A. Green, M. C. Hersam, A. V. Soldatov, Probing structural stability of double-walled carbon nanotubes at high non-hydrostatic pressure by raman spectroscopy, High Pressure Res. 31 (1) (2011) 186–190. arXiv:http://www.tandfonline.com/doi/pdf/10.1080/08957959.2011.562897, doi:10.1080/08957959.2011.562897.

[59] R. S. Alencar, W. Cui, A. C. Torres-Dias, T. F. T. Cerqueira, S. Botti, M. A. L. Marques, et al., Pressure-induced radial collapse in few-wall

carbon nanotubes: A combined theoretical and experimental study, Carbon 125 (2017) 429 – 436. doi:10.1016/j.carbon.2017.09.044.

[60] H. Shima, M. Sato, Pressure-induced structural transitions in multi-walled carbon nanotubes, physica status solidi (a) 206 (10) (2009) 2228–2233.

[61] Y. Magnin, H. Amara, F. Ducastelle, A. Loiseau, C. Bichara, Entropy-driven stability of chiral single-walled carbon nanotubes, Science 362 (6411) (2018) 212–215.

[62] A. C. Torres-Dias, S. Cambré, W. Wenseleers, D. Machon, A. San-Miguel, Chirality-dependent mechanical response of empty and water-filled single-wall carbon nanotubes at high pressure, Carbon (2015) 442–541doi:10.1016/j.carbon.2015.08.032.

[63] M. H. F. Sluiter, Y. Kawazoe, Phase diagram of single-wall carbon nanotube crystals under hydrostatic pressure, Phys. Rev. B 69 (2004) 224111. doi:10.1103/PhysRevB.69.224111.

[64] G. Carrier, On the buckling of elastic rings, Journal of Mathematics and Physics 26 (1-4) (1947) 94–103.

[65] D. J. Carter, D. J. Dunstan, W. Just, O. F. Bandtlow, A. S. Miguel, Softening of the euler buckling criterion under discretisation of compliance (2020). arXiv:2011.14120.

[66] A. C. Torres-Dias, T. F. Cerqueira, W. Cui, M. A. Marques, S. Botti, D. Machon, et al., From mesoscale to nanoscale mechanics in single-wall carbon nanotubes, Carbon 123 (2017) 145 – 150.

[67] C.-C. Ling, Q.-Z. Xue, L.-Y. Chu, N.-N. Jing, X.-Y. Zhou, Radial collapse of carbon nanotubes without and with stone–wales defects under hydrostatic pressure, RSC Adv. 2 (2012) 12182–12189. doi:10.1039/C2RA21581K.
URL http://dx.doi.org/10.1039/C2RA21581K

[68] N. M. Pugno, J. A. Elliott, Buckling of peapods, fullerenes and nanotubes, Physica E: Low-dimensional Systems and Nanostructures 44 (6) (2012) 944 – 948. doi:http://dx.doi.org/10.1016/j.physe.2011.12.024.

URL http://www.sciencedirect.com/science/article/pii/S1386947712000021

[69] A. Ghedjatti, Y. Magnin, F. Fossard, G. Wang, H. Amara, E. Flahaut, et al., Structural properties of double-walled carbon nanotubes driven by mechanical interlayer coupling, ACS nano 11 (5) (2017) 4840–4847.

[70] O. V. Kharissova, B. I. Kharisov, Variations of interlayer spacing in carbon nanotubes, RSC Adv. 4 (2014) 30807–30815.

[71] X. Meng, B. Zhang, H. Li, F. Li, Z. Kang, M. Li, et al., A theoretical analysis on self-collapsing of nanotubes, International Journal of Solids and Structures 160 (2019) 51–58.

[72] Y. Han, K. C. Lai, A. Lii-Rosales, M. C. Tringides, J. W. Evans, P. A. Thiel, Surface energies, adhesion energies, and exfoliation energies relevant to copper-graphene and copper-graphite systems, Surface Science 685 (2019) 48–58.

[73] L. Girifalco, R. Lad, Energy of cohesion, compressibility, and the potential energy functions of the graphite system, The Journal of chemical physics 25 (4) (1956) 693–697.

[74] B. Aradi, B. Hourahine, T. Frauenheim, Dftb+, a sparse matrix-based implementation of the dftb method, J. Phys. Chem. A 111 (26) (2007) 5678–5684.

[75] S. J. Stuart, A. B. Tutein, J. A. Harrison, A reactive potential for hydrocarbons with intermolecular interactions, The Journal of chemical physics 112 (14) (2000) 6472–6486.

[76] Y. Magnin, G. Förster, F. Rabilloud, F. Calvo, A. Zappelli, C. Bichara, Thermal expansion of free-standing graphene: benchmarking semi-empirical potentials, Journal of Physics: Condensed Matter 26 (18) (2014) 185401.

[77] M. Motta, A. Moisala, I. A. Kinloch, A. H. Windle, High performance fibres from 'dog bone' carbon nanotubes, Advanced Materials 19 (21) (2007) 3721–3726.

[78] J.-C. Blancon, A. Ayari, L. Marty, N. Bendiab, A. San-Miguel, Electronic transport in individual carbon nanotube bundles under pressure, Journal of Applied Physics 114 (14) (2013) 143704.

[79] L. Guan, K. Suenaga, S. Iijima, Smallest carbon nanotube assigned with atomic resolution accuracy, Nano Letters 8 (2) (2008) 459–462.

[80] X. Zhao, Y. Liu, S. Inoue, T. Suzuki, R. Jones, Y. Ando, Smallest carbon nanotube is 3 å in diameter, Physical review letters 92 (12) (2004) 125502.

[81] K. Syassen, Ruby under pressure, High Pressure Research 28 (2) (2008) 75–126. arXiv:https://doi.org/10.1080/08957950802235640, doi:10.1080/08957950802235640.
URL https://doi.org/10.1080/08957950802235640

[82] J. Zang, A. Treibergs, Y. Han, F. Liu, Geometric constant defining shape transitions of carbon nanotubes under pressure, Phys. Rev. Lett. 92 (2004) 105501.

[83] O. V. Kharissova, B. I. Kharisov, Variations of interlayer spacing in carbon nanotubes, RSC Adv. 4 (2014) 30807–30815. doi:10.1039/C4RA04201H.
URL http://dx.doi.org/10.1039/C4RA04201H

[84] V. D. Blank, V. D. Churkin, B. A. Kulnitskiy, I. A. Perezhogin, A. N. Kirichenko, V. N. Denisov, et al., Phase diagram of carbon and the factors limiting the quantity and size of natural diamonds, Nanotechnology 29 (11) (2018) 115603. doi:10.1088/1361-6528/aaa857.
URL https://doi.org/10.1088/1361-6528/aaa857

[85] M. Amsler, J. A. Flores-Livas, L. Lehtovaara, F. Balima, S. A. Ghasemi, D. Machon, et al., Crystal structure of cold compressed graphite, Phys. Rev. Lett. 108 (2012) 065501.

[86] A. Merlen, P. Toulemonde, S. L. Floch, G. Montagnac, T. Hammouda, O. Marty, et al., High pressure-high temperature synthesis of diamond from single-wall pristine and iodine doped carbon nanotube bundles, Carbon 47 (7) (2009) 1643 – 1651. doi:https://doi.org/10.1016/j.carbon.2009.02.014.

[87] L. A. Chernozatonskii, Polymerized nanotube structures – new zeolites?, Chemical Physics Letters 297 (3) (1998) 257–260. doi:https://doi.org/10.1016/S0009-2614(98)01100-2.
URL https://www.sciencedirect.com/science/article/pii/S0009261498011002

[88] M. Hu, Z. Zhao, F. Tian, A. R. Oganov, Q. Wang, M. Xiong, et al., Compressed carbon nanotubes: A family of new multifunctional carbon allotropes, Scientific Reports 3 (1). doi:10.1038/srep01331.
URL https://doi.org/10.1038/srep01331

[89] E. Y. Pashkin, A. M. Pankov, B. A. Kulnitskiy, I. A. Perezhogin, A. R. Karaeva, V. Z. Mordkovich, et al., The unexpected stability of multiwall nanotubes under high pressure and shear deformation, Applied Physics Letters 109 (8) (2016) 081904. doi:10.1063/1.4961618.

[90] J. Prasek, J. Drbohlavova, J. Chomoucka, J. Hubalek, O. Jasek, V. Adam, et al., Methods for carbon nanotubes synthesis—review, J. Mater. Chem. 21 (2011) 15872–15884.

[91] D. Bolmatov, M. Zhernenkov, D. Zav'yalov, S. N. Tkachev, A. Cunsolo, Y. Q. Cai, The frenkel line: a direct experimental evidence for the new thermodynamic boundary, Scientific reports 5 (2015) 15850.

[92] P. A. Djondjorov, V. M. Vassilev, I. M. Mladenov, Analytic description and explicit parametrisation of the equilibrium shapes of elastic rings and tubes under uniform hydrostatic pressure, International Journal of Mechanical Sciences 53 (5) (2011) 355–364.

[93] J. Frenzel, A. F. Oliveira, H. A. Duarte, T. Heine, G. Seifert, Structural and electronic properties of bulk gibbsite and gibbsite surfaces, Zeitschrift für anorganische und allgemeine Chemie 631 (6-7) (2005) 1267–1271.

[94] G. Zheng, S. Irle, K. Morokuma, Performance of the DFTB method in comparison to DFT and semiempirical methods for geometries and energies of c20–c86 fullerene isomers, Chemical Physics Letters 412 (1-3) (2005) 210–216. doi:10.1016/j.cplett.2005.06.105.
URL https://doi.org/10.1016/j.cplett.2005.06.105

[95] S. Plimpton, Fast parallel algorithms for short-range molecular dynamics, Journal of computational physics 117 (1) (1995) 1–19.

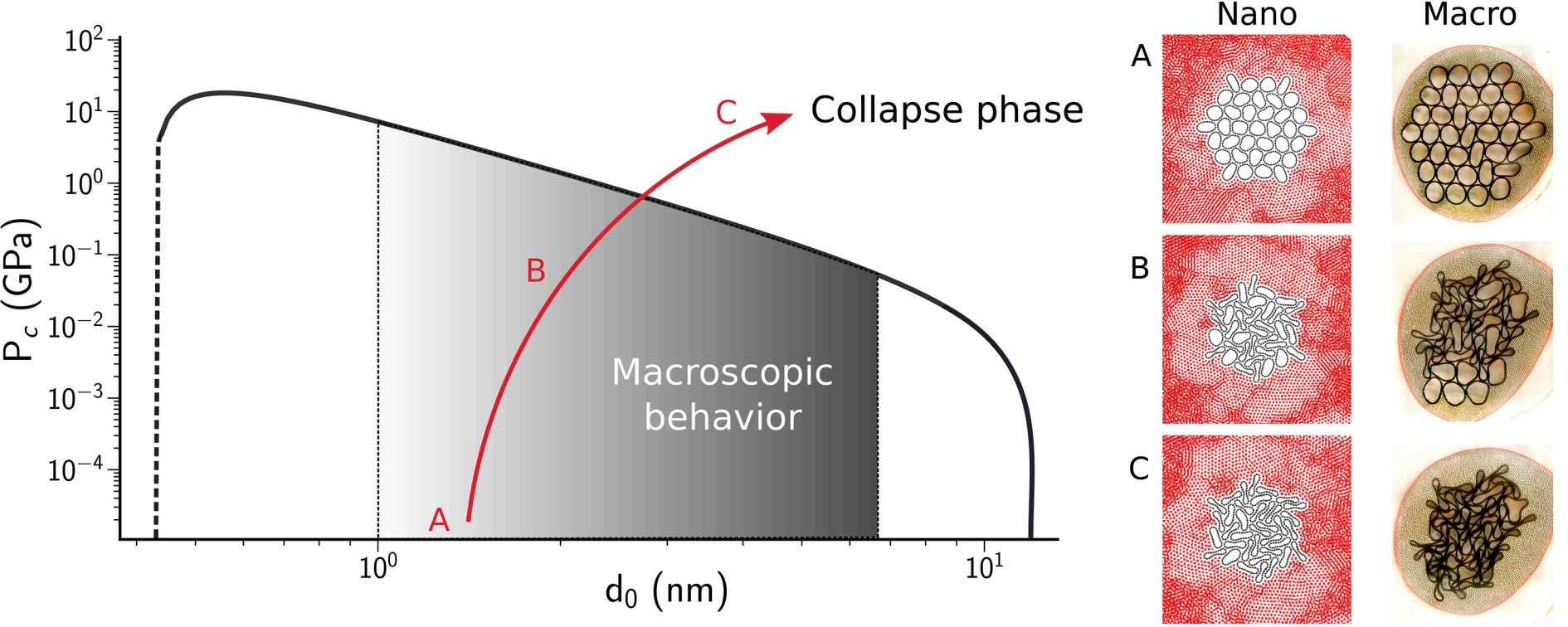
Nano
Macro
A
B
C
Collapse phase
Macroscopic behavior
P_c (GPa)
d_0 (nm)
10^2
10^1
10^0
10^{-1}
10^{-2}
10^{-3}
10^{-4}
10^0
10^1